

Neural Architecture Search using Covariance Matrix Adaptation Evolution Strategy

Nilotpal Sinha, Kuan-Wen Chen, *Member, IEEE*

Abstract—Evolution-based neural architecture search requires high computational resources, resulting in long search time. In this work, we propose a framework of applying the Covariance Matrix Adaptation Evolution Strategy (CMA-ES) to the neural architecture search problem called CMANAS, which achieves better results than previous evolution-based methods while reducing the search time significantly. The architectures are modelled using a normal distribution, which is updated using CMA-ES based on the fitness of the sampled population. We used the accuracy of a trained one shot model (OSM) on the validation data as a prediction of the fitness of an individual architecture to reduce the search time. We also used an architecture-fitness table (AF table) for keeping record of the already evaluated architecture, thus further reducing the search time. CMANAS finished the architecture search on CIFAR-10 with the top-1 test accuracy of 97.44% in 0.45 GPU day and on CIFAR-100 with the top-1 test accuracy of 83.24% for 0.6 GPU day on a single GPU. The top architectures from the searches on CIFAR-10 and CIFAR-100 were then transferred to ImageNet, achieving the top-5 accuracy of 92.6% and 92.1%, respectively.

Index Terms—Covariance matrix adaptation evolution strategy (CMA-ES), one shot model, neural architecture search.

I. INTRODUCTION

IN the recent years, convolutional neural networks (CNNs) have been very instrumental in solving various computer vision problems. However, the CNN architectures (such as AlexNet [1], ResNet [2], DenseNet [3], VGGNet [4]) have been designed mainly by humans, relying on their intuition and understanding of specific problem. *Neural architecture search* (NAS) tries to replace the reliance on human intuition with an automated search of the neural architecture. Recent NAS methods [5] [6] [7] have shown promising results in the field of computer vision but most of these methods consume a huge amount of computational power. Any NAS method has three parts (Fig. 1): *sampling* process, *evaluation* process and *update* process. The epoch in the NAS algorithm begins with sampling architecture from a given search space (i.e. sampling process), which is then sent to the evaluation process for the performance evaluation. On the basis of the evaluation metric, the NAS algorithm will update the sampling process (i.e. update process) in order to sample better performing architecture in the next epoch. The algorithm stops upon satisfying a stopping criterion.

Evolutionary algorithm (EA)-based NAS samples a population of architectures during the sampling process, which is updated during the update process on the basis of performance of the architectures from the evaluation process. Reinforcement learning (RL)-based NAS has a RL agent sampling architecture during the sampling process, which is updated

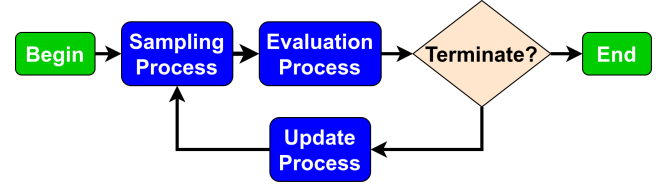


Fig. 1. Abstract illustration of Neural Architecture Search methods.

during the update process depending on the performance of the architecture determined by the evaluation process. Both types of methods require huge computational resources, resulting in long search time. For example, the method proposed in [8] required 3150 GPU days of evolution and that discussed in [9] required 1800 GPU days of RL search. This is attributed to the evaluation process wherein each architecture is trained from scratch for a certain number of epochs in order to evaluate its performance on the validation data. Recently proposed gradient-based methods such as [10] [11] [12] [13] [14] have reduced the search time by sharing weights among the architectures. However, these gradient-based methods highly depend on the given search space and suffer from premature convergence to the local optimum as shown in [14] [15].

In this work, we propose a method called CMANAS (*Neural Architecture using Covariance Matrix Adaptation Evolution Strategy*) which is summarized in Fig. 2. Here, the neural architecture is represented by a *normal distribution*. In every epoch, the distribution is first used to sample a population of architectures (i.e. sampling process) and then the distribution is updated using the covariance matrix adaptation evolution strategy (CMA-ES) [16] (i.e. update process) on the basis of the performance of the population of architectures (i.e. evaluation process). We used a trained *one shot model* (OSM) to evaluate each architecture instead of training each architecture from scratch. This resulted in reduced search time because of the weight sharing among all the architectures in the one shot model. We also used an architecture-fitness table (AF table) to maintain a record of the already evaluated architectures, which further resulted in reducing the search time.

Our contributions could be summarized as follows:

- We designed a framework of applying the covariance matrix adaptation evolution strategy to the NAS problem with reduced computational requirements by using a trained one shot model for evaluating the performance/fitness of an architecture. The architectures are modelled by a multivariate normal distribution, which is updated using CMA-ES depending on the fitness

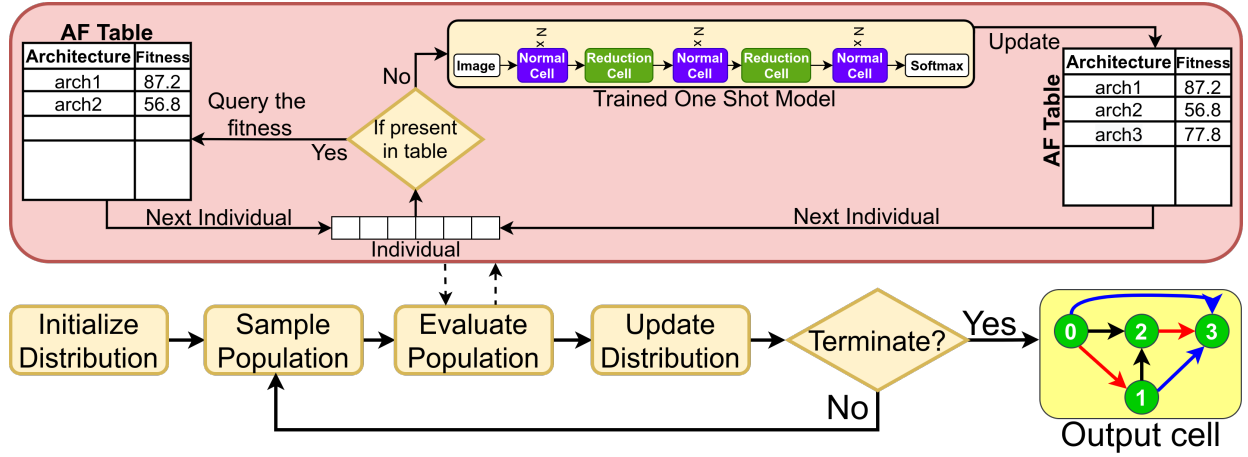


Fig. 2. Illustration of the general framework of CMANAS.

- estimated by the trained OSM.
- We used an architecture-fitness table (AF table) for maintaining the records of the already evaluated architectures in order to skip the process of re-evaluating an already evaluated architecture and thus reducing the search time.
- We applied our method to two different search spaces to show that CMANAS is search space independent (i.e. search space agnostic) as is not the case for the gradient-based NAS methods.
- We also created a visualization of the architecture search performed by CMANAS to get insights into the search process. We found that the first phase of the search is predominantly an *exploration* phase wherein CMANAS explores the given search space. This is followed by an *exploitation* phase (i.e. convergence to an architecture).

II. RELATED WORK

Searching the neural architecture automatically by using an algorithm (i.e. NAS) is an alternative to the architectures designed by humans, and in the recent years, these NAS methods have attracted increasing interest because of its promise of an automatic and efficient search of architectures specific to a task. Early NAS approaches [17] [18] optimized both the neural architectures and the weights of the network using evolution. However, their usage was limited to shallow networks. Recent NAS methods [6] [7] [8] [9] [19] [20] [21] perform the architecture search separately while using gradient descent for optimizing the weights of the architecture for its evaluation. This has made possible the search of deep networks. The various NAS methods can be classified into two categories on the basis of the different methods used in the update process in Fig. 1. These are *gradient-based* methods and *non-gradient based* methods.

Gradient-Based Methods: These methods begin with a random neural architecture, which can be regarded as the sampling process in Fig. 1. The neural architecture is then updated using the gradient information on the basis of its performance on the validation data (i.e. update process in Fig. 1). In general, these methods [10] [11] [12] [13] relax

the discrete architecture search space to a continuous search space by using an one shot model (OSM). The performance of the OSM on the validation data is used for updating the architecture using gradients. As the OSM shares weights among all architectures in the search space, these methods take lesser time in the evaluation process in Fig. 1 and thus shorter search time. However, these methods suffer from the overfitting problem wherein the resultant architecture shows good performance on the validation data but exhibits poor performance on the test data. This can be attributed to its preference for parameter-less operations in the search space, as it leads to rapid gradient descent [14]. Some regularization techniques have been introduced to tackle this problem, such as early stopping [15], search space regularization [14] and architecture refinement [14]. In contrast to these gradient-based methods, our method does not suffer from the overfitting problem because of its stochastic nature.

Non-Gradient Based Methods: These methods include reinforcement learning (RL) methods and evolutionary algorithm (EA) methods. In the RL methods, an agent is used for the generating neural architecture (i.e. sampling process in Fig. 1). The agent is then trained (i.e. update process in Fig. 1) to generate architectures in order to maximize its expected accuracy on the validation data (calculated in the evaluation process in Fig. 1). In [6] [9], a recurrent neural network (RNN) is used as an agent for sampling the neural architectures. These sampled architectures are then trained from scratch to convergence in order to get their accuracies on the validation data (i.e. evaluation process in Fig. 1). These accuracies are then used for updating the weights of the RNN agent by using policy gradient methods. Because of the huge computational requirement of training the architectures from scratch in the evaluation process, both of these methods suffered from long search time. This was improved in [7] by using a single directed acyclic graph (DAG) for sharing the weights among all the sampled architectures, thus resulting in reduced computational resources.

The EA based NAS methods begin with a population of architectures which can be regarded as the sampling process

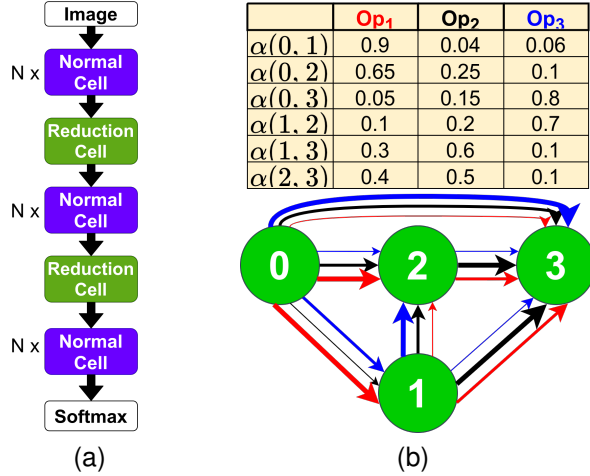


Fig. 3. (a) Architecture created by stacking cells. (b) Architecture representation (α) of a cell in the one shot model with three different operations $Op(\cdot)$ in the search space \mathcal{O} . The colors of the arrows between any two nodes represent the different operations and the thickness of the arrow is proportional to the weight of the corresponding operation.

in Fig. 1. Each architecture in the population is evaluated on the basis of its performance on the validation data (evaluation process in Fig. 1). The population is then evolved (i.e. update process in Fig. 1) on the basis of the performance of the population. Methods such as those proposed in [8] [21] used gradient descent for optimizing the weights of each architecture in the population from scratch in order to determine their accuracies on the validation data as their fitness during the evaluation process, resulting in huge computational requirements. In order to speed up the training process, in [19], the authors introduced weight inheritance wherein the architectures in the post-update process population inherit the weights of the pre-update process population, resulting in bypassing the training from scratch. However, the speed up gained is less as it still needs to optimize the weights of the architecture. Methods such as that proposed in [22] use a random forest for predicting the performance of the architecture during the evaluation process, resulting in a high speed up as compared to previous EA methods. However, its performance was far from the state-of-the-art results. In contrast, our method achieved better results than previous EA methods while using significantly less computational resources. CMA-ES has shown good performance in many high-dimensional continuous optimization problems such as fine-tuning the hyperparameters of the CNN [23]. However, to the best of our knowledge, CMA-ES has not been applied to the NAS problem because of the discrete nature of the problem.

III. PROPOSED APPROACH

A. Search Space

The choice of the search space can affect the quality of the searched architecture. CMANAS searches for both operations and connections which is in contrast to previous EA-based NAS [21] [22] [24] [25], focusing on one facet of the architecture search, e.g. connections and/or hyper-parameters. This makes our search space more comprehensive. The success of

the recent hand-crafted CNN architectures is attributed to their sharing similar characteristics of repeating motifs [2] [3] [26]. Therefore, in [9] [27], the researchers proposed to search for such motifs called cells, instead of the whole architecture. In this work, we used this cell-based search space, which has been successfully employed in recent works [7] [8] [9] [10] [11] [13] [28] [29] and allows us to be consistent with these works. As illustrated in Fig 3(a), the architecture is created by stacking together cells of two types: *normal* cells which preserve the dimensionality of the input with a stride of one and *reduction* cells which reduce the spatial dimension with a stride of two.

To construct both types of cells, we used *directed acyclic graphs* (DAGs) containing n nodes and edge (i, j) between any two nodes representing an operation from the search space with N_{ops} different operations. In this work, we applied our method to two different search spaces: *Search space 1 (S1)* [10] and *Search space 2 (S2)* [30]. In S1, we search for both normal and reduction cells where each node $x^{(j)}$ maps two inputs to one output. The two inputs for $x^{(j)}$ in cell k are picked from the outputs from previous nodes $x^{(i)}$ in cell k (i.e. $i < j$), output from previous cell c_{k-1} and output from the previous-to-previous cell c_{k-2} . In S2, we search for only normal cells, where each node $x^{(j)}$ is connected to the previous node $x^{(i)}$ (i.e. $i < j$).

B. Representation of Architecture

Evaluating an architecture involves training it from scratch for some epochs and then evaluating it on the basis of its performance on validation data, leading to a long search time [8] [9]. Instead, we used a *one shot model (OSM)* [10], which shares the weights among all architectures by treating all the architectures as the subgraphs of a supergraph. As illustrated in Fig 3(b), a cell in the one shot model is represented by an *architecture parameter*, α . It represents the weights of different operations $Op(\cdot)$ in the given operation space \mathcal{O} (i.e. the search space of NAS) between a pair of nodes where each $Op(\cdot)$ represents some function to be applied to some node $x^{(i)}$. In OSM, the directed edge from node i to node j is the weighted sum of all $Op(\cdot)$ s in \mathcal{O} where the $Op(\cdot)$ s are weighted by normalized $\alpha^{(i,j)}$ using softmax. This can be written as:

$$f^{(i,j)}(x^{(i)}) = \sum_{Op \in \mathcal{O}} \frac{\exp(\alpha_{Op}^{(i,j)})}{\sum_{Op' \in \mathcal{O}} \exp(\alpha_{Op'}^{(i,j)})} Op(x^{(i)}) \quad (1)$$

where $\alpha_{Op}^{(i,j)}$ represents the weight of the operation $Op(\cdot)$ in the operation space \mathcal{O} between node i and node j . Each α for a normal cell and a reduction cell is represented by a matrix (Fig. 3(b)) with columns representing the weights of different operations $Op(\cdot)$ s from the operation space \mathcal{O} and rows representing the edge between two nodes. This design choice allows us to skip the individual architecture training from scratch for its evaluation because of the weight-sharing nature of OSM, thus resulting in a significant reduction of search time. As discussed in Section III-A, an architecture is derived from α for the two search spaces through a *mapping* process in the following ways:

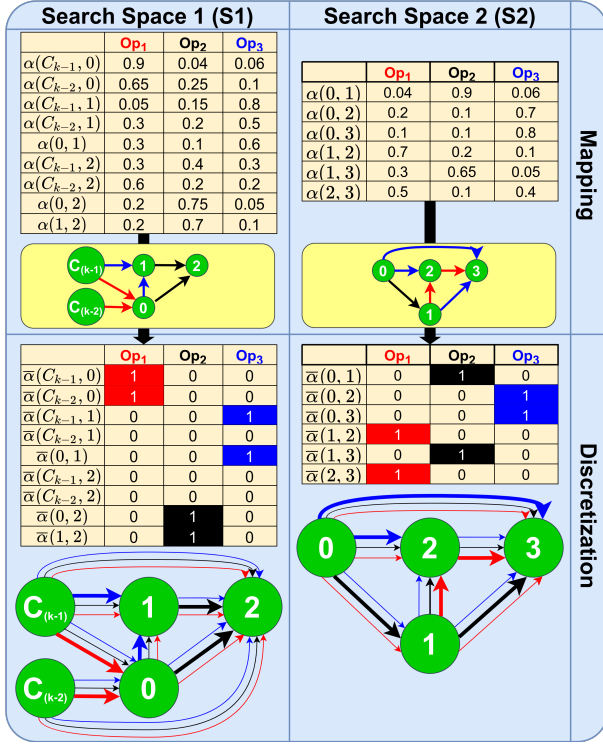


Fig. 4. Process of evaluating architecture using the trained one shot model with three nodes for S1 and four nodes for S2. *Top*: mapping process wherein the architecture parameter α is mapped to its corresponding architecture. c_{k-1} and c_{k-2} refer to outputs from the previous cell and previous-to-previous cell respectively. *Bottom*: discretization process wherein $\hat{\alpha}$ is created from the derived architecture and is copied to the ONS. The colors of the arrows between any two nodes represent the different operations and the thickness of the arrow is proportional to the weight of the corresponding operation.

- *Search space 1 (S1)*: For each node, the top two distinct input nodes are chosen from all previous nodes on the basis of the weights of all the operations in the search space.
- *Search space 2 (S2)*: For each edge between any two nodes, the top operation is chosen on the basis of weights of all the operations in the search space.

Fig. 4 illustrates the mapping process with three operations in both S1 and S2 and three nodes in S1 and four nodes in S2.

C. Performance Estimation

The performance of an architecture is calculated by the trained one shot model using the validation data. The OSM is trained for a certain number of epochs using *Stochastic Gradient Descent* (SGD [31]) with momentum. The training of the OSM begins with randomly initializing the weights of the OSM. Then for each training batch in an epoch, the architecture parameter, α of the OSM is updated to random values (as shown in Fig. 5) so that no particular sub-graph (i.e. architecture) receives most of the gradient updates of the super-graph (i.e. OSM). The algorithm is summarized in Algorithm 1 and its implementation details discussed in Section IV-C2.

The trained OSM from Algorithm 1 is then used to evaluate an architecture on the basis of its accuracy on the validation

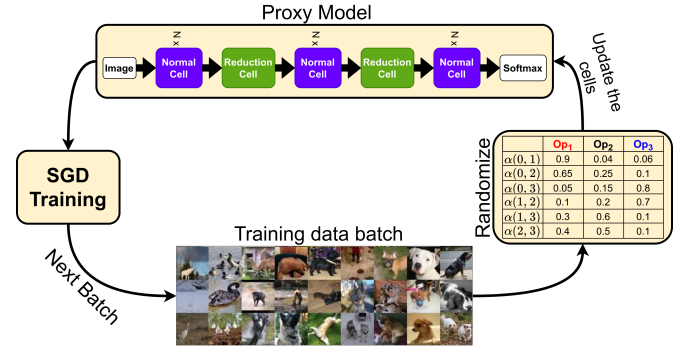


Fig. 5. Abstract illustration of training the one shot model in an epoch.

Algorithm 1: Training one shot model

Input: One shot model M , architecture parameter α , training data \mathcal{D}_{tr} , total epochs N_{epochs} , initial learning rate η_{max} , minimum learning rate η_{min} , weight decay λ , momentum ρ .

Output: Trained one shot model M .

- 1 $W \leftarrow$ Randomly initialize weights of M ;
- 2 $\Delta v \leftarrow 0$ (Initialize the momentum term);
- 3 **for** $\tau \leftarrow 1$ **to** N_{epochs} **do**
- 4 $\eta_\tau \leftarrow \eta_\tau + \frac{1}{2}(\eta_{max} - \eta_{min})(1 + \cos(\frac{\tau}{N_{epochs}}\pi))$;
- 5 **for each batch** (\mathcal{B}) **in** \mathcal{D}_{tr} **do**
- 6 $\alpha \leftarrow$ Update to random values;
- 7 $\hat{W} \leftarrow W - \eta_\tau \cdot \rho \cdot \Delta v$;
- 8 $\mathcal{L}(\hat{W}, \mathcal{B}) \leftarrow$ Cross-entropy on the batch;
- 9 $\Delta v \leftarrow \rho \cdot \Delta v + (1 - \rho) \cdot \nabla_W \mathcal{L}(\hat{W}, \mathcal{B})$;
- 10 $W \leftarrow (1 - \lambda)W - \eta_\tau \Delta v$;
- 11 **end**
- 12 **end**

data, also known as the *fitness* of the architecture. The process of evaluation follows two steps sequentially (as illustrated in Fig. 4):

- *Mapping* process: Here, the architecture, \mathcal{A} , is derived from the architecture parameter α , on the basis of the search space used (Section III-B).
- *Discretization* process: The derived architecture is then used to create a new architecture parameter called *discrete architecture* parameter, $\bar{\alpha}$ with the following entries:

$$\bar{\alpha}_{Op}^{(i,j)} = \begin{cases} 1, & \text{if } Op(x^{(i)}) \text{ present in } \mathcal{A} \\ 0, & \text{otherwise} \end{cases} \quad (2)$$

$\bar{\alpha}$ is then copied to the OSM for evaluating its accuracy on the validation data, which is the *fitness* of the architecture \mathcal{A} .

D. CMA-ES

Covariance matrix adaptation evolution strategy (CMA-ES) [16] is a state-of-the-art evolutionary algorithm for continuous blackbox functions (i.e. functions for which only the function values are available for the search points [32]). We used the capability of CMA-ES's convergence to find a solution

Algorithm 2: CMANAS

Input: Trained one shot model M , validation data \mathcal{D}_{va} , total generations N_{gen} , population size N_{pop} .

Output: Searched architecture, $\mathbf{m}^{(N_{gen})}$.

```

1  $g \leftarrow 0$  (Initialize the epoch counter);
2 Initialize CMA-ES with  $\mathbf{m}^{(g)} \leftarrow \vec{0}$ ,  $\mathbf{C}^{(g)} \leftarrow \mathbf{I}$  and  $\sigma^{(g)}$ ;
3 while  $g \leq N_{gen}$  do
4   Sample population,  $\mathcal{P}$ , of  $N_{pop}$  individuals using Eq. 3;
5   for each individual architecture ( $\mathcal{A}$ ) in  $\mathcal{P}$  do
6     if  $\mathcal{A}$  already present in AF table then
7        $fitness(\mathcal{A}) \leftarrow$  entry in the AF table;
8     else
9        $fitness(\mathcal{A}) \leftarrow$  Evaluate  $\mathcal{A}$  using  $M$ ;
10      Insert  $fitness(\mathcal{A})$  to the AF table;
11    end
12  end
13  Update  $\mathbf{m}^{(g)}$ ,  $\sigma^{(g)}$  and  $\mathbf{C}^{(g)}$  using Eq. 4, Eq. 5, Eq. 6 in CMA-ES;
14   $g \leftarrow g + 1$ ;
15 end

```

using small population size, as compared to other evolutionary methods, for reducing the search time.

For N_{ops} number of operations in the search space and N_{edges} edges between nodes in the cell, α has $N_{ops} \times N_{edges}$ parameters. These are modelled with a multivariate normal distribution $\mathcal{N}(\mathbf{m}, \mathbf{C})$ with a mean vector, \mathbf{m} , of size $N_{ops} \times N_{edges}$, representing the parameters in α , and a covariance matrix, \mathbf{C} , of size $(N_{ops} \times N_{edges}) \times (N_{ops} \times N_{edges})$. CMANAS is an iterative process, where in each iteration/generation, a population of architectures (i.e. α) with the population size N_{pop} is sampled from the normal distribution $\mathcal{N}(\mathbf{m}, \mathbf{C})$ according to the following equation:

$$\alpha_{1:N_{pop}}^{(g+1)} \sim \mathbf{m}^{(g)} + \sigma^{(g)} \mathcal{N}(0, \mathbf{C}^{(g)}) \quad (3)$$

where $g = 0, 1, 2, \dots$ is the generation number and σ is the step-size. The fitness of the individual architecture in the population is then evaluated using the trained OSM model (Section III-C), and the architectures are sorted in the decreasing order according to their fitness. The top- μ individuals are used to update the mean, \mathbf{m} , as follows:

$$\mathbf{m}^{(g+1)} \leftarrow \sum_{i=1}^{\mu} w_i \alpha_i^{(g+1)} \quad (4)$$

where $\mu = N_{pop}/2$ and this process is also referred to as the *selection* and *recombination* part of CMA-ES. The step-size, σ , is then updated using a *conjugate evolution path*, p_σ which is calculated as the sum of the previous successive steps taken over a number of generations. Its length is compared with the expected length under random selection in order to decide whether to increase or decrease the σ , as follows:

$$\sigma^{(g+1)} \leftarrow \sigma^{(g)} \times \exp \left(\frac{c_\sigma}{d_\sigma} \left(\frac{\|p_\sigma^{(g)}\|}{E\|\mathcal{N}(0, \mathbf{I})\|} - 1 \right) \right) \quad (5)$$

where c_σ and d_σ are the hyperparameters of CMA-ES. Lastly, the covariance matrix, \mathbf{C} , is updated using two terms: *Rank- μ update*, ($Rank_\mu$) and *Rank-1 update*, ($Rank_1$). $Rank_\mu$ is calculated using the previous generation covariance matrices with higher weights given to recent generations. The $Rank_1$ is calculated using another evolution path which is expressed as a sum of consecutive steps taken over a number of generations. The whole process is summarized as follows:

$$\mathbf{C}^{(g+1)} \leftarrow (1+k)\mathbf{C}^{(g)} + c_1 Rank_1^{(g)} + c_\mu Rank_\mu^{(g)} \quad (6)$$

where k, c_1 and c_μ are the hyperparameters of CMA-ES. For a more detailed analysis of the hyperparameters and the updates in CMA-ES, please refer to [32].

E. CMANAS

As illustrated in Fig. 2, CMANAS starts with initializing the normal distribution $\mathcal{N}(\mathbf{m}, \mathbf{C})$. This distribution is then used to sample a population of architectures (using Eq. (3)), which are then evaluated using the trained OSM. In the evaluation process, we use an architecture-fitness table (AF table) to save the fitness of the already evaluated architecture. For an individual architecture in the population, we first check whether there is an entry present in the AF table for this architecture. If it is already present, then the entry in the AF table is returned. Otherwise, the fitness of the architecture is evaluated using the trained OSM (Section III-C), and the AF table is updated with it. The normal distribution $\mathcal{N}(\mathbf{m}, \mathbf{C})$ and the step-size, σ , are updated using CMA-ES according to the evaluated population. The updated distribution is then re-sampled for the next generation population of architectures and repeat the cycle for a certain number of generations, N_{gen} . The mean of the normal distribution is returned as the searched architecture, $\mathbf{m}^{(N_{gen})}$ after N_{gen} generations. The algorithm is summarized in Algorithm 2.

IV. EXPERIMENTS AND RESULTS

A. Baselines

In order to illustrate the effectiveness of CMANAS, we compared the architecture returned by CMANAS with the other architectures reported in various peer-reviewed NAS methods. These peer-reviewed NAS methods are broadly classified into five categories: architectures designed by human (reported as *manual*), RL based methods (reported as *RL*), gradient-based methods (reported as *grad. based*), EA based methods (reported as *EA*) and *others*. The *others* include the random search [33] and sequential model-based optimization (SMBO) wherein the architecture is searched in the increasing order of complexity of its structure. The effectiveness of the reported architectures are measured in terms of the classification accuracy and the computational requirement, measured in terms of search time on a single GPU reported as GPU days.

B. Dataset Settings

Both **CIFAR-10** and **CIFAR-100** [34] have 50K training images and 10K testing images and are classified into 10 classes and 100 classes respectively. **ImageNet** [35] is a

popular benchmark for image classification and contains 1.28 million training images and 50K images test images, which are classified into 1K classes. **ImageNet-16-120** [36] is a down-sampled version of ImageNet wherein the images in the original ImageNet dataset are downsampled to 16×16 pixels with 120 classes to construct the ImageNet-16-120 dataset. The settings used for the datasets in **S1** are as follows:

- **CIFAR-10**: We followed [10] and split 50K training images into two sets of size 25K each, with one set acting as the training set and the other set as the validation set.
- **CIFAR-100**: We followed [28] and split 50K training images into two sets. One set of size 40K images becomes the training set and the other set of size 10K images becomes the validation set.

We followed the settings used in [30] for the datasets in **S2** which are as follows:

- **CIFAR-10**: The same settings as those used for S1 is used here as well.
- **CIFAR-100**: The 50K training images remains as the training set and the 10K testing images are split into two sets of size 5K each, with one set acting as the validation set and the other set as the test set.
- **ImageNet-16-120**: It has 151.7K training images, 3K validation images and 3K test images.

The training set is used for training the OSM (Fig. 5) and the validation set is used for estimating the fitness of the sampled architecture during the search process (Section III-C).

C. Implementation Details

1) **Search Space 1 (S1)**: This is similar to that used in DARTS [10], which allows us to compare the performance of CMANAS with other NAS methods. Here, we search for both normal and reduction cells in Fig. 3(a) wherein each cell has seven nodes with first two nodes being the output from previous cells and last node as output node, resulting in 14 edges among them. There are eight operations considered in S1 which are as follows: 3×3 and 5×5 dilated separable convolutions, 3×3 and 5×5 separable convolutions, 3×3 max pooling, 3×3 average pooling, skip connect and zero. Therefore, an architecture is represented by two 14×8 matrices, one each for a normal cell and a reduction cell. The values in these two matrices are modelled with a multivariate normal distribution $\mathcal{N}(\mathbf{m}, \mathbf{C})$ with a mean vector, \mathbf{m} , of size 224, and a covariance matrix, \mathbf{C} , of size 224×224 .

2) **Search Space 2 (S2)**: This is a smaller search space with a total of 15,625 architectures in the search space and is similar to that used in NAS-Bench-201 [30], where we only search for the normal cell in Figure 3(a). NAS-Bench-201 provides a unified benchmark for almost any up-to-date NAS algorithms by providing the results of each architecture in the search space on CIFAR-10, CIFAR-100 and ImageNet16-120. It provides an API that can be used to query accuracies on both validation and test sets for all the architectures in the search space. The API provides two types of accuracies for each architecture, i.e. accuracy after training the architecture for 12 epochs and 200 epochs. The accuracies of the architectures after 200 epochs are used as the performance measurement of various NAS

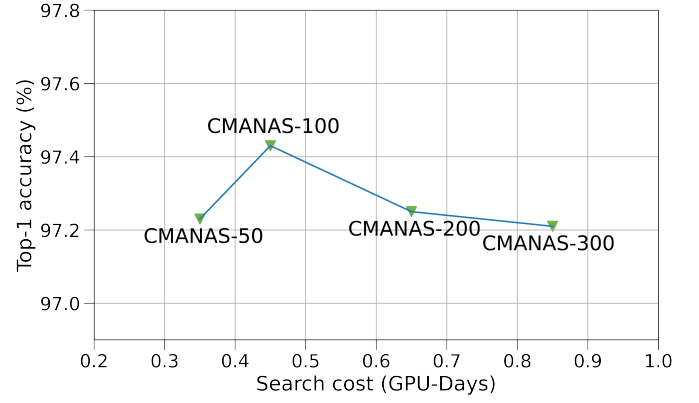


Fig. 6. Top1 accuracy of architecture searches performed with OSM trained for 50, 100, 200 and 300 epochs in S1 on CIFAR-10 dataset. The number after CMANAS specifies the number of epochs.

algorithms. NAS-Bench-201 [30] (i.e. S2) provides the search results for two types of NAS methods: *weight sharing* based and *non-weight sharing* based. In the weight sharing based NAS methods, all the architectures in the search space share their weights to reduce the search time (e.g. [7] [10] [11] [13] [33]). In the non-weight sharing based NAS methods (e.g. [8] [37] [38] [39]), the architectures in the search space do not share their weights, and during the architecture search, the performance of each architecture is evaluated on the basis of the accuracy on the validation data after training for 12 epochs which is provided by the API.

Here, each cell has four nodes with the first node as the input node and last node as the output node, resulting in six edges among them. The five operations considered in S2 are as follows: 1×1 and 3×3 convolutions, 3×3 average pooling, skip connect and zero. Therefore, an architecture is represented by a 6×5 matrix for the normal cell. The values in the matrix are modelled with a multivariate normal distribution, $\mathcal{N}(\mathbf{m}, \mathbf{C})$, with a mean vector, \mathbf{m} , of size 30, and a covariance matrix, \mathbf{C} , of size 30×30 .

3) **Training Settings**: The training process is executed two times in our method which are as follows:

- **One shot model (OSM) training**: In general, the OSM suffers from high memory requirements which makes it difficult to fit it in a single GPU. For S1, we follow [10] [33] and use a smaller OSM, called *proxy model* which is created with 8 stacked cells and 16 initial channels. It is then trained with SGD for 100 epochs on both CIFAR-10 and CIFAR-100 with the same settings i.e. batch size of 96, weight decay $\lambda = 3 \times 10^{-4}$, cutout [40], initial learning rate $\eta_{max} = 0.025$ (annealed down to 0 by using a cosine schedule without restart [41]) and momentum $\rho = 0.9$. For S2, we do not use a proxy model as the size of the OSM is sufficiently small to be fitted in a single GPU. For training, we follow the same settings as those used in S1 for CIFAR-10, CIFAR-100 and ImageNet16-120 except batch size of 256.
- **Architecture evaluation**: Here, the discovered architecture, \mathcal{A} (i.e. discovered cells), at the end of the archi-

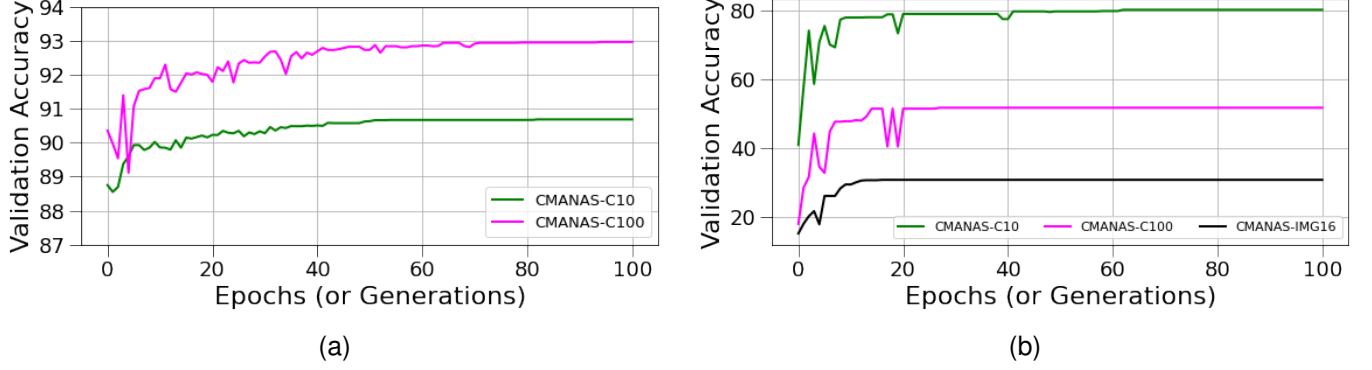


Fig. 7. Plot of validation accuracy/fitness of the mean, \mathbf{m} , of the normal distribution, $\mathcal{N}(\mathbf{m}, \mathbf{C})$ at each epoch/generation in (a) S1 on CIFAR-10 (denoted as CMANAS-C10) and CIFAR-100 (denoted as CMANAS-C100). (b) S2 on CIFAR-10 (denoted as CMANAS-C10), CIFAR-100 (denoted as CMANAS-C100) and ImageNet16-120 (denoted as CMANAS-IMG16). All the plots are averaged over all three runs in both S1 and S2.

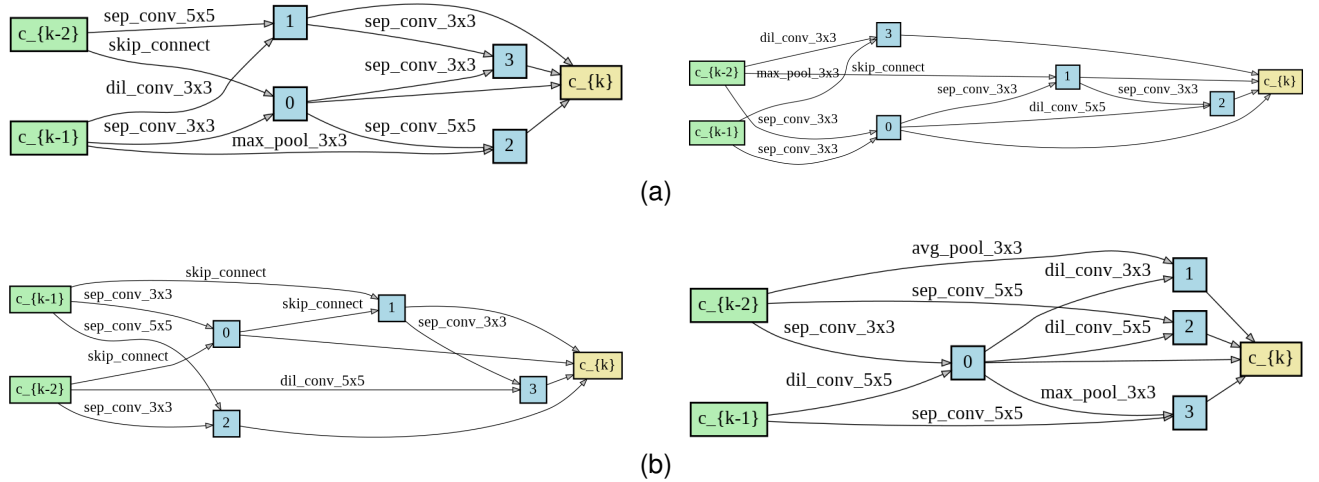


Fig. 8. Normal cell on the left side and reduction cell in the right side. (a) Cells discovered by CMANAS-C10A (b) Cells discovered by CMANAS-C100A

texture search is trained on the dataset to evaluate its performance for comparing with other NAS methods. For *S1*, we follow the training settings used in DARTS [10]. Here, \mathcal{A} is created with 20 stacked cells and 36 initial channels for both CIFAR-10 and CIFAR-100 datasets. It is then trained for 600 epochs on both the datasets with the same settings as the ones used in the OSM training above. Following recent works [7] [8] [9] [10] [29], we use an auxiliary tower with 0.4 as its weights, path dropout probability of 0.2 and cutout [40] for additional enhancements. For ImageNet, \mathcal{A} is created with 14 cells and 48 initial channels in the mobile setting, wherein the input image size is 224 x 224 and the number of multiply-add operations in the model is restricted to less than 600M. It is trained on 8 NVIDIA V100 GPUs by following the training settings used in [14].

All the above trainings were performed on a single Nvidia RTX 3090 GPU except the one on ImageNet. The number of epochs for training the ONS was chosen to be 100 as we found that the performance of the architecture search increases from 50 epochs to 100 epochs and then deteriorates upon further increase in the number of epochs because of the overfitting of the OSM (as shown in Fig. 6).

4) Architecture Search Settings: The multivariate normal distribution, $\mathcal{N}(\mathbf{m}, \mathbf{C})$, that is used to model the architecture parameter, α , is initialized with its mean, \mathbf{m} equal to the zero vector. This results in the assignment of equal weights to all the operations in all the edges because of the normalization by softmax (Eq. 1). As recommended in [32], we initialize the covariance matrix, \mathbf{C} , with an identity matrix and the population size, N_{pop} to $4 + \lfloor 3 \times \ln(n) \rfloor$, where n is the size of the mean, \mathbf{m} . Therefore, for *S1*, $N_{pop} = 20$ and for *S2*, $N_{pop} = 14$. The other hyperparameters of CMA-ES are initialized to their default values as per the recommendation in [32]. We run CMANAS for 100 epochs/generations as we observed that the algorithm converged well before 100 epochs for both *S1* and *S2* (as shown in Fig. 7). All the architecture searches were performed on a single Nvidia RTX 3090 GPU. All the codes were implemented using the deep learning framework, PyTorch [42].

D. Results

1) Search Space 1 (S1): We performed three architecture searches on CIFAR-10 with different random number seeds; their results are provided in Table I(a) as CMANAS-C10A, CMANAS-C10B and CMANAS-C10C. We also per-

TABLE I

COMPARISON OF CMANAS WITH OTHER NAS METHODS IN S1 IN TERMS OF TEST ACCURACY (HIGHER IS BETTER) ON (A) CIFAR-10 (B) CIFAR-100 AND (C) IMAGENET.

Architecture	Top-1 Acc. (%)	Params (M)	GPU Days	Search Method
ResNet [2]	95.39	1.7	-	manual
DenseNet-BC [3]	96.54	25.6	-	manual
PNAS [29]	96.59	3.2	225	SMBO
RSPS [33]	97.14	4.3	2.7	random
NASNet-A [9]	97.35	3.3	1800	RL
ENAS [7]	97.14	4.6	0.45	RL
DARTS [10]	97.24	3.3	4	grad. based
GDAS [11]	97.07	3.4	0.83	grad. based
SNAS [12]	97.15	2.8	1.5	grad. based
SETN [13]	97.31	4.6	1.8	grad. based
AmoebaNet-A [8]	96.66	3.2	3150	EA
Large-scale Evo. [19]	94.60	5.4	2750	EA
Hierarchical Evo. [20]	96.25	15.7	300	EA
CNN-GA [43]	96.78	2.9	35	EA
CGP-CNN [25]	94.02	1.7	27	EA
AE-CNN [44]	95.7	2.0	27	EA
NSGANetV1-A2 [28]	97.35	0.9	27	EA
AE-CNN+E2EPP [22]	94.70	4.3	7	EA
NSGA-NET [45]	97.25	3.3	4	EA
CMANAS-C10A	97.44	3.8	0.45	EA
CMANAS-C10B	97.35	3.2	0.45	EA
CMANAS-C10C	97.35	3.3	0.45	EA
CMANAS-C10rand	97.11	3.11	0.66	random

(a) CIFAR-10

Architecture	Top-1 Acc. (%)	Params (M)	GPU Days	Search Method
ResNet [2]	77.90	1.7	-	manual
DenseNet-BC [3]	82.82	25.6	-	manual
PNAS [29]	80.47	3.2	225	SMBO
MetaQNN [46]	72.86	11.2	90	RL
ENAS [7]	80.57	4.6	0.45	RL
DARTS [10]	82.46	3.3	4	grad. based
GDAS [11]	81.62	3.4	0.83	grad. based
SETN [13]	82.75	4.6	1.8	grad. based
AmoebaNet-A [8]	81.07	3.2	3150	EA
Large-scale Evo. [19]	77.00	40.4	2750	EA
CNN-GA [43]	79.47	4.1	40	EA
AE-CNN [44]	79.15	5.4	36	EA
NSGANetV1-A2 [28]	82.58	0.9	27	EA
Genetic CNN [21]	70.95	-	17	EA
AE-CNN+E2EPP [22]	77.98	20.9	10	EA
NSGA-NET [45]	79.26	3.3	8	EA
CMANAS-C100A	83.24	3.4	0.60	EA
CMANAS-C100B	83.09	3.47	0.63	EA
CMANAS-C100C	82.73	2.97	0.62	EA
CMANAS-C100rand	82.35	3.17	0.67	random

(b) CIFAR-100

Architecture	Test Accuracy (%)		Params (M)	+× (M)	Search Time (GPU Days)	Search Method
	top 1	top 5				
MobileNet-V2 [47]	72.0	91.0	3.4	300	-	manual
PNAS [29]	74.2	91.9	5.1	588	225	SMBO
NASNet-A [9]	74.0	91.6	5.3	564	1800	RL
NASNet-B [9]	72.8	91.3	5.3	488	1800	RL
NASNet-C [9]	72.5	91.0	4.9	558	1800	RL
DARTS [10]	73.3	91.3	4.7	574	4	grad. based
GDAS [11]	74.0	91.5	5.3	581	0.83	grad. based
SNAS [12]	72.7	90.8	4.3	522	1.5	grad. based
SETN [13]	74.3	92.0	5.4	599	1.8	grad. based
AmoebaNet-A [8]	74.5	92.0	5.1	555	3150	EA
AmoebaNet-B [8]	74.0	91.5	5.3	555	3150	EA
AmoebaNet-C [8]	75.7	92.4	6.4	570	3150	EA
NSGANetV1-A2 [28]	74.5	92.0	4.1	466	27	EA
CMANAS-C10A	75.3	92.6	5.3	589	0.45	EA
CMANAS-C100A	74.8	92.1	4.8	531	0.60	EA

(c) ImageNet

formed another three architecture search on CIFAR-100 with different random number seeds; their results are provided in Table I(b) as CMANAS-C100A, CMANAS-C100B and CMANAS-C100C. The results show that the cells discovered by CMANAS on CIFAR-10 and CIFAR-100 achieve better results than those by human designed, RL based, gradient based and EA based methods while using significantly less computational time. We compared the computation time (or *search cost*) spent on the *GPU days*, of CMANAS with that for the other NAS methods (as shown in Fig. 9). GPU days for any NAS method is calculated by multiplying the number of GPUs used in the NAS method by the execution time (reported in units of days). A single run of CMANAS on CIFAR-10 and CIFAR-100 took 0.45 and 0.6 GPU days (including the training time of the OSM and the architecture search time using the trained OSM on the dataset), respectively. For comparison with other NAS methods, the search cost on

CIFAR-10 for CMANAS was used, as it is the most common search cost used in most of the NAS methods. From Fig. 9, we observe that CMANAS is able to achieve better results than the previous evolution based methods AmoebaNet [8], Large-scale Evolution [19] and Hierarchical Evolution [20] while using **10x** to **1000x** less GPU days. The top cells discovered by CMANAS on CIFAR-10 and CIFAR-100 (i.e. CMANAS-C10A, CMANAS-C100A) are shown in Fig. 8. The cells discovered by the other runs of CMANAS on CIFAR-10 and CIFAR-100 are provided in the supplementary.

We followed [7] [8] [9] [10] [29] to compare the transfer capability of CMANAS with that of the other NAS methods, wherein the discovered architecture on a dataset was transferred to another dataset (i.e. ImageNet) by retraining the architecture from scratch on the new dataset. The best discovered architectures from the architecture search on CIFAR-10 and CIFAR-100 (i.e. CMANAS-C10A and CMANAS-

TABLE II

COMPARISON OF CMANAS WITH OTHER NAS METHODS ON NAS-BENCH-201 (I.E. S2) [30] WITH MEAN \pm STD. ACCURACIES ON CIFAR-10, CIFAR-100 AND ImageNet16-120 (HIGHER IS BETTER). THE FIRST BLOCK COMPARES CMANAS WITH OTHER WEIGHT SHARING BASED NAS METHODS. THE SECOND BLOCK COMPARES CMANAS WITH OTHER NON-WEIGHT SHARING BASED NAS METHODS. OPTIMAL IN THE THIRD BLOCK REFERS TO THE BEST ARCHITECTURE ACCURACY FOR EACH DATASET. SEARCH TIMES ARE GIVEN FOR A CIFAR-10 SEARCH ON A SINGLE GPU.

Method	Search (seconds)	CIFAR-10		CIFAR-100		ImageNet-16-120		Search Method
		validation	test	validation	test	validation	test	
RSPS [33]	7587.12	84.16 \pm 1.69	87.66 \pm 1.69	59.00 \pm 4.60	58.33 \pm 4.64	31.56 \pm 3.28	31.14 \pm 3.88	random
DARTS-V1 [10]	10889.87	39.77 \pm 0.00	54.30 \pm 0.00	15.03 \pm 0.00	15.61 \pm 0.00	16.43 \pm 0.00	16.32 \pm 0.00	grad. based
DARTS-V2 [10]	29901.67	39.77 \pm 0.00	54.30 \pm 0.00	15.03 \pm 0.00	15.61 \pm 0.00	16.43 \pm 0.00	16.32 \pm 0.00	grad. based
GDAS [11]	28925.91	90.00 \pm 0.21	93.51 \pm 0.13	71.14 \pm 0.27	70.61 \pm 0.26	41.70 \pm 1.26	41.84 \pm 0.90	grad. based
SETN [13]	31009.81	82.25 \pm 5.17	86.19 \pm 4.63	56.86 \pm 7.59	56.87 \pm 7.77	32.54 \pm 3.63	31.90 \pm 4.07	grad. based
ENAS [7]	13314.51	39.77 \pm 0.00	54.30 \pm 0.00	15.03 \pm 0.00	15.61 \pm 0.00	16.43 \pm 0.00	16.32 \pm 0.00	RL
CMANAS	13896	89.06 \pm 0.4	92.05 \pm 0.26	67.43 \pm 0.42	67.81 \pm 0.15	39.54 \pm 0.91	39.77 \pm 0.57	EA
AmoebaNet [8]	0.02	91.19 \pm 0.31	93.92 \pm 0.30	71.81 \pm 1.12	71.84 \pm 0.99	45.15 \pm 0.89	45.54 \pm 1.03	EA
RS [37]	0.01	90.93 \pm 0.36	93.70 \pm 0.36	70.93 \pm 1.09	71.04 \pm 1.07	44.45 \pm 1.10	44.57 \pm 1.25	random
REINFORCE [38]	0.12	91.09 \pm 0.37	93.85 \pm 0.37	71.61 \pm 1.12	71.71 \pm 1.09	45.05 \pm 1.02	45.24 \pm 1.18	RL
BOHB [39]	3.59	90.82 \pm 0.53	93.61 \pm 0.52	70.74 \pm 1.29	70.85 \pm 1.28	44.26 \pm 1.36	44.42 \pm 1.49	grad. based
CMANAS-h12-Ep25	3.64	91.23 \pm 0.40	94.00 \pm 0.39	72.16 \pm 1.19	72.11 \pm 1.10	45.69 \pm 0.84	45.7 \pm 0.79	EA
CMANAS-h12-Ep100	7.12	91.28 \pm 0.35	94.06 \pm 0.34	72.40 \pm 0.96	72.26 \pm 0.84	45.74 \pm 0.86	45.69 \pm 0.88	EA
ResNet	N/A	90.83	93.97	70.42	70.86	44.53	43.63	manual
Optimal	N/A	91.61	94.37	73.49	73.51	46.77	47.31	N/A

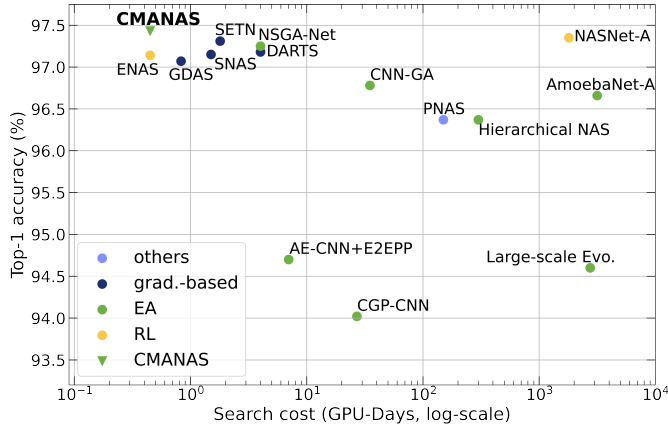


Fig. 9. Search cost comparison of CMANAS with the other NAS algorithms in S1.

C100A) were then evaluated on the ImageNet dataset in mobile setting and the results are provided in Table I(c). The results show that the cells discovered by CMANAS on CIFAR-10 and CIFAR-100 can be successfully transferred to ImageNet, achieving better results than those of human designed, RL based, gradient based and EA based methods while using significantly less computational time.

2) *Search Space 2 (S2)*: We performed architecture search on the CIFAR-10, CIFAR-100 and ImageNet-16-120 datasets for both the types of NAS methods given in S2 [30]:

- *Weight sharing based NAS*: Here, the architecture evaluation in CMANAS used the trained OSM (as discussed in Section III-C). Following [30], we perform the architecture search three times on all the three datasets and compared the results with those of other weight sharing based NAS methods because of the weight sharing nature of the OSM. The results are reported as CMANAS in Table II.
- *Non-Weight sharing based NAS*: Here, the fitness of the architecture was evaluated to be the accuracy on the

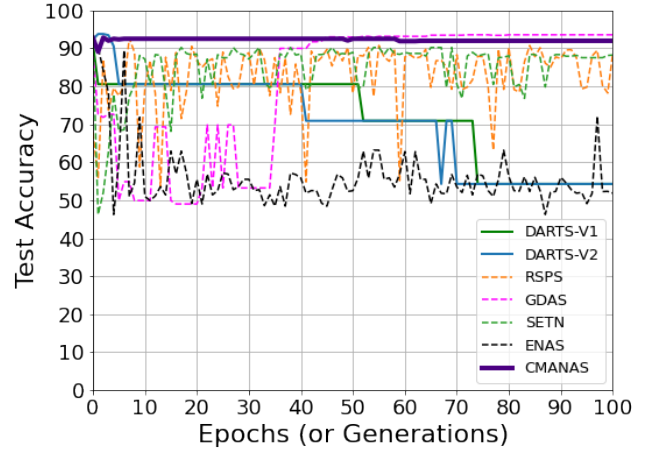


Fig. 10. Comparison of the weight sharing based CMANAS with other weight sharing based NAS methods in terms of the test accuracy of the derived architecture evaluated on CIFAR-10 at each epoch for the search space S2.

validation data after training for 12 epochs, which is provided by the API in S2. Following [30], we performed the architecture search 500 times on all the three datasets for 25 epochs each and compared the results with those of the other non-weight sharing based NAS methods; the corresponding results are reported as CMANAS-h12-Ep25 in Table II. We also performed another architecture search 500 times on all the three datasets for 100 epochs each and reported the corresponding results as CMANAS-h12-Ep100 in Table II; we found no significant improvement over the 25 epoch version.

The results show that CMANAS outperforms most of the weight sharing NAS methods except GDAS [11]. However, GDAS performs worse when the size of the search space increases as can be seen for S1 in Table I. CMANAS also dominates the non-weight sharing based NAS methods. Notably, the non-weight sharing based CMANAS (i.e. CMANAS-h12-

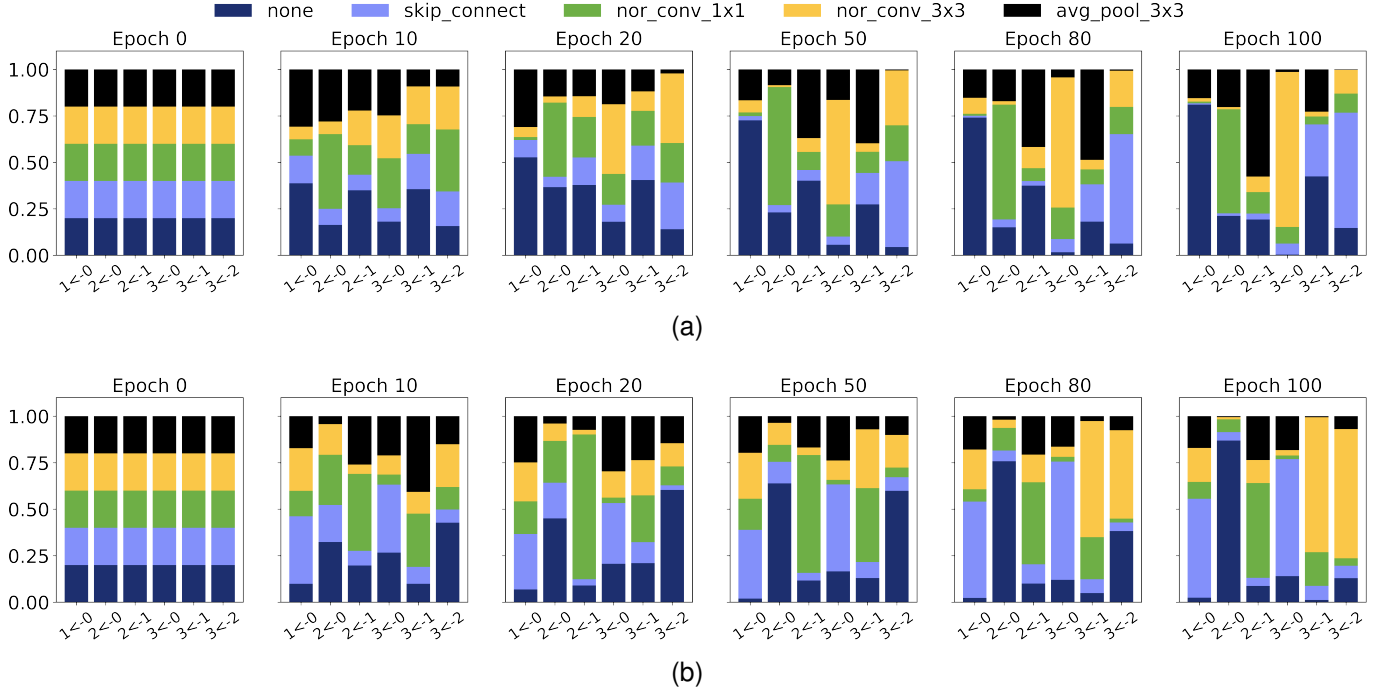


Fig. 11. Visualizing the progression of the mean of the normal distribution $\mathcal{N}(\mathbf{m}, \mathbf{C})$. The colors represent the operations in S2 and the width of the color is directly proportional to the weight of the operation associated with that color for that specific edge (x -axis). All the searches were performed on CIFAR-10 for the search space S2. (a) Architecture search with weight sharing based CMANAS. (b) Architecture search with non weight sharing based CMANAS.

Ep25) also dominates the weight sharing based CMANAS, which shows that the trained OSM provides a noisy estimate of the fitness/performance of an architecture.

CMANAS vs Gradient-Based methods: In Fig. 10, we compare the progression of the search of the weight sharing based CMANAS with that of the other weight sharing based NAS methods. The gradient-based method like DARTS [10] suffers from overfitting problem wherein it converges to operations that give faster gradient descent, i.e. *skip-connect* operation due to its parameter-less nature as reported in [14] [15] [30]. This leads to higher number of *skip-connect* in the final discovered cell, a local optimum (as shown in Fig. 10). In contrast, CMANAS does not get stuck to a local optimum architecture due to its stochastic nature.

V. FURTHER ANALYSIS

In the following sections, we will analyze the different aspects of CMANAS.

A. Visualizing the Architecture Search

For analyzing the search, we visualize the search process by using the following techniques:

- We plotted the number of unique architectures sampled in every epoch for both weight sharing based CMANAS and non-weight sharing based NAS (i.e. CMANAS-h12-Ep100) in S2 for CIFAR-10 and the weight sharing based CMANAS in S1 for both CIFAR-10 and CIFAR-100 in Fig. 12. From the figure, we made the following observations:
 - 1) The number of unique architectures sampled in the beginning part of the architecture search was equal

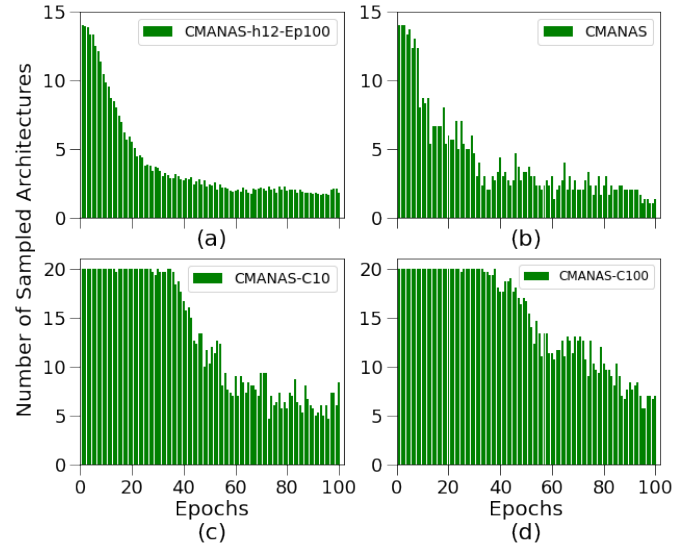


Fig. 12. Number of unique architectures sampled in every epoch averaged over all the runs. (a) Non-weight sharing based CMANAS for S2 on CIFAR-10. (b) Weight sharing based CMANAS for S2 on CIFAR-10. (c) CMANAS for S1 on CIFAR-10. (d) CMANAS for S1 on CIFAR-100.

to the population size, N_{pop} . This part could be considered as the *exploration* phase of CMANAS wherein the algorithm is exploring the search space by sampling unique architectures.

- 2) As the search progressed, the number of unique sampled architectures decreased because of the dominance of some architecture solutions in the population. This part could be considered as the

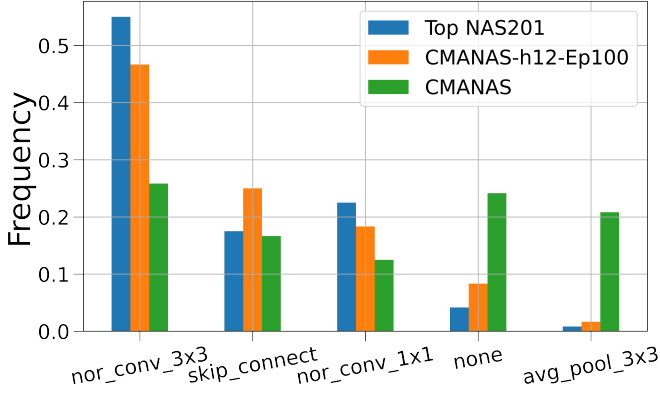


Fig. 13. Frequency of all operations in S2 for top-20 architectures in S2, (i.e. NAS-Bench-201 [30]) labeled as "Top NAS201", top-20 sampled architectures of non-weight sharing based CMANAS, labeled as "CMANAS-h12-Ep100", and top-20 sampled architectures of weight sharing based CMANAS, labeled as "CMANAS".

exploitation phase of CMANAS wherein the algorithm keeps on sampling the already evaluated good solution.

- 3) The non-weight sharing based CMANAS (i.e. CMANAS-h12-Ep100) converged considerably faster to a better solution than the weight sharing based CMANAS in S2. This showed that the trained OSM provided a noisy estimate of the fitness of the architecture.
- 4) Because of the bigger size of S1 than that of S2, the exploration phase of CMANAS was larger in S1 than in S2.

- As the architecture parameter, α , is modelled using the mean of the normal distribution $\mathcal{N}(\mathbf{m}, \mathbf{C})$, we can visualize the progression of α by visualizing the mean, \mathbf{m} , throughout the architecture search epochs. In Fig. 11, the mean, \mathbf{m} , of the distribution in an epoch is visualized using a bar plot wherein each bar in the plot represents the edge between two nodes in the cell (x -axis). All the operations in the search space are represented by different colors and the weight associated with any operation between two nodes (i.e. α) is represented by the width of the color associated with that operation in the bar associated with that specific edge. From the figure, we observed that the search began with equal weights to all the operations in all the edges at epoch 0, and as the search progressed, CMANAS changes the weights according to the fitness estimation of the architectures in the population. As the search converged to an architecture, CMANAS increased the weights of the operations of this architecture in the OSM. Fig. 11 shows the search progression for both weight sharing based CMANAS and non-weight sharing based CMANAS for S2 on CIFAR-10 dataset only. For CIFAR-100 and ImageNet16-120 datasets, please refer to the supplementary.

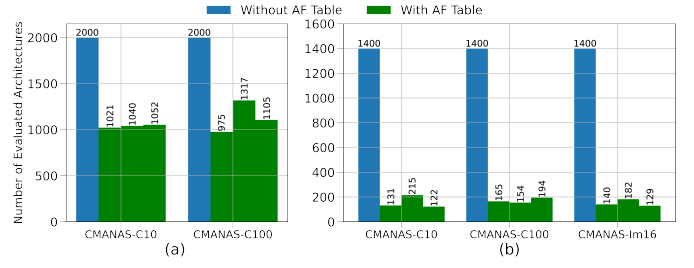


Fig. 14. Total number of architectures evaluated in a single run of weight sharing based CMANAS on (a) S1 for CIFAR-10 and CIFAR-100, (b) S2 for CIFAR-10, CIFAR-100 and ImageNet16-120.

B. Observation on Sampled Architectures

The API provided in the search space, S2, (i.e. NAS-Bench-201 [30]) allows a faster way to analyze a NAS algorithm. To discover the patterns associated with the sampled architectures, we plotted the frequency of all the operations in the search space S2 for the top-20 sampled architectures (in terms of their estimated fitness) in both the non-weight sharing based CMANAS (i.e. CMANAS-h12-Ep100) and the weight sharing based CMANAS in Fig. 13. They were compared with the frequency of all the operations in the search space S2 for the top-20 architectures (in terms of the test accuracy after 200 epochs), for S2, and we observed the following:

- The operation 3×3 convolutions dominated the top-20 architectures of S2 which was also seen in the non-weight sharing based CMANAS, but the weight sharing based CMANAS showed a marginal dominance.
- The frequency of operation 3×3 average pooling was very low in the top-20 architectures of S2 and was also seen in the non-weight sharing based CMANAS, but the weight sharing based CMANAS showed higher frequency.

All these show that the trained OSM provides a noisy estimate of the fitness of the architecture and with a better estimator, CMANAS can yield better results.

C. Ablation

Comparison with Random Search: Here, we do not the update the normal distribution, $\mathcal{N}(\mathbf{m}, \mathbf{C})$, after estimating the fitness of the individual architectures in the population (i.e. no "update distribution" block in Fig. 2). The sampled architecture with the best fitness is returned as the searched architecture after 100 epochs. This is essentially a random search and is reported in Table I for CIFAR-10 as CMANAS-C10rand and for CIFAR-100 as CMANAS-C100rand. We found that CMANAS-C10rand shows similar results to those reported in RSPS [33] (random search with parameter sharing). We also found that the CMANAS took less time than the random search for both datasets while outperforming the random search in both the datasets.

Effectiveness of the AF Table: To illustrate the effectiveness of the AF table used during the evaluation of the fitness of the architecture, we plotted the total number of architectures

TABLE III
SEARCH TIME OF CMANAS WITH AND WITHOUT THE AF TABLE IN BOTH S1 AND S2.

	S1		S2		
	Search time in GPU days		Search time in seconds		
	CIFAR-10	CIFAR-100	CIFAR-10	CIFAR-100	ImageNet16-120
Without AF table	0.66	0.67	21807	27648	14220
With AF table	0.45	0.62	13824	25992	13536

evaluated during the CMANAS search with and without AF table in Fig 14, and made the following observations:

- On average, the use of the AF table reduces the architecture evaluation by half for S1 and by one-tenth for S2. This results in reducing the search time for CMANAS in both the search spaces on all the datasets and has been summarized in Table III.
- Because of the smaller size of S2 than that of S1, CMANAS requires smaller number of architecture evaluations in order to converge to an optimal solution in S2 than in S1.
- The speedup is much bigger for CIFAR-10 as compared to the other datasets in both S1 and S2 because of the bigger size of the validation data used for CIFAR-10 (Section IV-B), which results in longer fitness evaluation time.

VI. CONCLUSION AND FUTURE WORK

The goal of this paper was to develop a framework for applying the Covariance Matrix Adaptation Evolution Strategy to the NAS problem while using significantly less computational time than the previous evolution based NAS methods. This was achieved by using a trained one shot model (OSM) for evaluating the architectures in the population. The OSM shares weights among all the architectures in the search space, which allows us to skip training each individual architecture from scratch for its fitness evaluation. This leads to reduced search time. We applied CMANAS to two different search spaces to show its effectiveness in generalizing to any cell-based search space, i.e. search space agnostic. Experimentally, CMANAS reduced the search time of evolution based architecture search significantly by 10x to 1000x, while achieving better results on CIFAR-10, CIFAR-100 and ImageNet datasets than the previous evolutionary algorithms. CMANAS also solves the overfitting problem present in the gradinet-based NAS method because of its stochastic nature. We also analyzed the search process and found that the first part of the architecture search in the CMANAS acts as the exploration phase, wherein it explores the search space, and the later part acts as the exploitation phase, wherein the search converges to an architecture.

A possible future direction to improve the performance of the algorithm is to use a better fitness estimator as we found that a better estimator would allow CMANAS to achieve its full potential.

ACKNOWLEDGMENT

This work was supported in part by the Ministry of Science and Technology of Taiwan (MOST 108-2221-E-009-067-MY3

and MOST 110-2634-F-009-018-). Furthermore, we are grateful to the National Center for High-performance Computing for computer time and facilities.

REFERENCES

- [1] A. Krizhevsky, I. Sutskever, and G. E. Hinton, "Imagenet classification with deep convolutional neural networks," in *Advances in Neural Information Processing Systems*, 2012, pp. 1097–1105.
- [2] K. He, X. Zhang, S. Ren, and J. Sun, "Deep residual learning for image recognition," in *Proceedings of the IEEE Conference on Computer Vision and Pattern Recognition*, 2016, pp. 770–778.
- [3] G. Huang, Z. Liu, L. Van Der Maaten, and K. Q. Weinberger, "Densely connected convolutional networks," in *Proceedings of the IEEE Conference on Computer Vision and Pattern Recognition*, 2017, pp. 4700–4708.
- [4] K. Simonyan and A. Zisserman, "Very deep convolutional networks for large-scale image recognition," *arXiv preprint arXiv:1409.1556*, 2014.
- [5] T. Elsken, J. H. Metzen, and F. Hutter, "Neural architecture search: A survey," *arXiv preprint arXiv:1808.05377*, 2018.
- [6] B. Zoph and Q. V. Le, "Neural architecture search with reinforcement learning," *arXiv preprint arXiv:1611.01578*, 2016.
- [7] H. Pham, M. Guan, B. Zoph, Q. Le, and J. Dean, "Efficient neural architecture search via parameters sharing," in *Proceedings of the 35th International Conference on Machine Learning*, ser. Proceedings of Machine Learning Research, J. Dy and A. Krause, Eds., vol. 80. Stockholm: PMLR, 10–15 Jul 2018, pp. 4095–4104. [Online]. Available: <http://proceedings.mlr.press/v80/pham18a.html>
- [8] E. Real, A. Aggarwal, Y. Huang, and Q. V. Le, "Regularized evolution for image classifier architecture search," in *Proceedings of the AAAI Conference on Artificial Intelligence*, vol. 33, 2019, pp. 4780–4789.
- [9] B. Zoph, V. Vasudevan, J. Shlens, and Q. V. Le, "Learning transferable architectures for scalable image recognition," in *Proceedings of the IEEE Conference on Computer Vision and Pattern Recognition*, 2018, pp. 8697–8710.
- [10] H. Liu, K. Simonyan, and Y. Yang, "DARTS: Differentiable architecture search," in *International Conference on Learning Representations*, 2019. [Online]. Available: <https://openreview.net/forum?id=S1eYHoC5FX>
- [11] X. Dong and Y. Yang, "Searching for a robust neural architecture in four gpu hours," in *Proceedings of the IEEE Conference on computer vision and pattern recognition*, 2019, pp. 1761–1770.
- [12] S. Xie, H. Zheng, C. Liu, and L. Lin, "SNAS: stochastic neural architecture search," in *International Conference on Learning Representations*, 2019. [Online]. Available: <https://openreview.net/forum?id=rylqooRqK7>
- [13] X. Dong and Y. Yang, "One-shot neural architecture search via self-evaluated template network," in *Proceedings of the IEEE International Conference on Computer Vision*, 2019, pp. 3681–3690.
- [14] X. Chen, L. Xie, J. Wu, and Q. Tian, "Progressive differentiable architecture search: Bridging the depth gap between search and evaluation," in *Proceedings of the IEEE International Conference on Computer Vision*, 2019, pp. 1294–1303.
- [15] A. Zela, T. Elsken, T. Saikia, Y. Marrakchi, T. Brox, and F. Hutter, "Understanding and robustifying differentiable architecture search," in *International Conference on Learning Representations*, 2020. [Online]. Available: <https://openreview.net/forum?id=H1gDNyrKDS>
- [16] N. Hansen and A. Ostermeier, "Completely derandomized self-adaptation in evolution strategies," *Evolutionary computation*, vol. 9, no. 2, pp. 159–195, 2001.
- [17] K. O. Stanley and R. Miikkulainen, "Evolving neural networks through augmenting topologies," *Evolutionary Computation*, vol. 10, no. 2, pp. 99–127, 2002.
- [18] K. O. Stanley, D. B. D'Ambrosio, and J. Gauci, "A hypercube-based encoding for evolving large-scale neural networks," *Artificial life*, vol. 15, no. 2, pp. 185–212, 2009.
- [19] E. Real, S. Moore, A. Selle, S. Saxena, Y. L. Suematsu, J. Tan, Q. V. Le, and A. Kurakin, "Large-scale evolution of image classifiers," in *Proceedings of the 34th International Conference on Machine Learning-Volume 70*. JMLR.org, 2017, pp. 2902–2911.
- [20] H. Liu, K. Simonyan, O. Vinyals, C. Fernando, and K. Kavukcuoglu, "Hierarchical representations for efficient architecture search," in *International Conference on Learning Representations*, 2018. [Online]. Available: <https://openreview.net/forum?id=BJQRKzbA->
- [21] L. Xie and A. Yuille, "Genetic cnn," in *Proceedings of the IEEE International Conference on Computer Vision*, 2017, pp. 1379–1388.

- [22] Y. Sun, H. Wang, B. Xue, Y. Jin, G. G. Yen, and M. Zhang, "Surrogate-assisted evolutionary deep learning using an end-to-end random forest-based performance predictor," *IEEE Transactions on Evolutionary Computation*, vol. 24, no. 2, pp. 350–364, 2019.
- [23] I. Loshchilov and F. Hutter, "Cma-es for hyperparameter optimization of deep neural networks," *arXiv preprint arXiv:1604.07269*, 2016.
- [24] T. Elsken, J. H. Metzen, and F. Hutter, "Efficient multi-objective neural architecture search via lamarckian evolution," *arXiv preprint arXiv:1804.09081*, 2018.
- [25] M. Suganuma, S. Shirakawa, and T. Nagao, "A genetic programming approach to designing convolutional neural network architectures," in *Proceedings of the genetic and evolutionary computation conference*, 2017, pp. 497–504.
- [26] C. Szegedy, V. Vanhoucke, S. Ioffe, J. Shlens, and Z. Wojna, "Rethinking the inception architecture for computer vision," in *Proceedings of the IEEE conference on computer vision and pattern recognition*, 2016, pp. 2818–2826.
- [27] Z. Zhong, J. Yan, W. Wu, J. Shao, and C.-L. Liu, "Practical block-wise neural network architecture generation," in *Proceedings of the IEEE conference on computer vision and pattern recognition*, 2018, pp. 2423–2432.
- [28] Z. Lu, I. Whalen, Y. Dhebar, K. Deb, E. Goodman, W. Banzhaf, and V. N. Boddeti, "Multi-objective evolutionary design of deep convolutional neural networks for image classification," *IEEE Transactions on Evolutionary Computation*, 2020.
- [29] C. Liu, B. Zoph, M. Neumann, J. Shlens, W. Hua, L.-J. Li, F.-F. Li, A. Yuille, J. Huang, and K. Murphy, "Progressive neural architecture search," in *Proceedings of the European Conference on Computer Vision (ECCV)*, 2018, pp. 19–34.
- [30] X. Dong and Y. Yang, "Nas-bench-201: Extending the scope of reproducible neural architecture search," in *International Conference on Learning Representations*, 2020. [Online]. Available: <https://openreview.net/forum?id=HJxyZkBKDr>
- [31] I. Sutskever, J. Martens, G. Dahl, and G. Hinton, "On the importance of initialization and momentum in deep learning," in *International conference on machine learning*. PMLR, 2013, pp. 1139–1147.
- [32] N. Hansen, "The cma evolution strategy: A tutorial," *arXiv preprint arXiv:1604.00772*, 2016.
- [33] L. Li and A. Talwalkar, "Random search and reproducibility for neural architecture search," in *Uncertainty in Artificial Intelligence*. PMLR, 2020, pp. 367–377.
- [34] A. Krizhevsky, G. Hinton *et al.*, "Learning multiple layers of features from tiny images," 2009.
- [35] J. Deng, W. Dong, R. Socher, L. Li, Kai Li, and Fei-Fei Li, "Imagenet: a large-scale hierarchical image database," in *2009 IEEE Conference on Computer Vision and Pattern Recognition*, 2009, pp. 248–255.
- [36] P. Chrabaszcz, I. Loshchilov, and F. Hutter, "A downsampled variant of imagenet as an alternative to the cifar datasets," *arXiv preprint arXiv:1707.08819*, 2017.
- [37] J. Bergstra and Y. Bengio, "Random search for hyper-parameter optimization," *Journal of machine learning research*, vol. 13, no. 2, 2012.
- [38] R. J. Williams, "Simple statistical gradient-following algorithms for connectionist reinforcement learning," *Machine learning*, vol. 8, no. 3-4, pp. 229–256, 1992.
- [39] S. Falkner, A. Klein, and F. Hutter, "Bohb: Robust and efficient hyperparameter optimization at scale," in *International Conference on Machine Learning*. PMLR, 2018, pp. 1437–1446.
- [40] T. DeVries and G. W. Taylor, "Improved regularization of convolutional neural networks with cutout," *arXiv preprint arXiv:1708.04552*, 2017.
- [41] I. Loshchilov and F. Hutter, "SGDR: stochastic gradient descent with warm restarts," in *5th International Conference on Learning Representations, ICLR 2017, Toulon, France, April 24-26, 2017, Conference Track Proceedings*. OpenReview.net, 2017. [Online]. Available: <https://openreview.net/forum?id=Skq89Scxx>
- [42] A. Paszke, S. Gross, F. Massa, A. Lerer, J. Bradbury, G. Chanan, T. Killeen, Z. Lin, N. Gimelshein, L. Antiga, A. Desmaison, A. Kopf, E. Yang, Z. DeVito, M. Raison, A. Tejani, S. Chilamkurthy, B. Steiner, L. Fang, J. Bai, and S. Chintala, "Pytorch: An imperative style, high-performance deep learning library," in *Advances in Neural Information Processing Systems* 32, H. Wallach, H. Larochelle, A. Beygelzimer, F. d'Alché-Buc, E. Fox, and R. Garnett, Eds. Curran Associates, Inc., 2019, pp. 8024–8035. [Online]. Available: <http://papers.neurips.cc/paper/9015-pytorch-an-imperative-style-high-performance-deep-learning-library.pdf>
- [43] Y. Sun, B. Xue, M. Zhang, G. G. Yen, and J. Lv, "Automatically designing cnn architectures using the genetic algorithm for image classification," *IEEE transactions on cybernetics*, vol. 50, no. 9, pp. 3840–3854, 2020.
- [44] Y. Sun, B. Xue, M. Zhang, and G. G. Yen, "Completely automated cnn architecture design based on blocks," *IEEE transactions on neural networks and learning systems*, vol. 31, no. 4, pp. 1242–1254, 2019.
- [45] Z. Lu, I. Whalen, V. Boddeti, Y. Dhebar, K. Deb, E. Goodman, and W. Banzhaf, "Nsga-net: neural architecture search using multi-objective genetic algorithm," in *Proceedings of the Genetic and Evolutionary Computation Conference*, 2019, pp. 419–427.
- [46] B. Baker, O. Gupta, N. Naik, and R. Raskar, "Designing neural network architectures using reinforcement learning," *International Conference on Learning Representations*, 2017.
- [47] M. Sandler, A. Howard, M. Zhu, A. Zhmoginov, and L.-C. Chen, "Mobilenetv2: Inverted residuals and linear bottlenecks," in *Proceedings of the IEEE conference on computer vision and pattern recognition*, 2018, pp. 4510–4520.